Title: **Establishment and validation of surface model for biodosimetry based on γ-H2AX foci detection**

Authors: Juan S. López[a], Mònica Pujol-Canadell[a], Pedro Puig[b,c], Montserrat Ribas[d], Pablo Carrasco[d], Gemma Armengol[a], Joan F. Barquinero[a*]

Affiliations:

[a] Unitat d'Antropologia Biològica, Departament de Biologia Animal, Biologia Vegetal i Ecologia, Universitat Autònoma de Barcelona, E-08193, Bellaterra, Catalonia, Spain.

[b] Departament de Matemàtiques, Universitat Autònoma de Barcelona, E-08193 Bellaterra, Catalonia, Spain

[c] Centre de Recerca Matemàtica, E-08193 Bellaterra, Catalonia, Spain.

[d] Servei de Radiofísica i Radioprotecció, Hospital de la Santa Creu i Sant Pau, Sant Antoni Maria Claret 167, Barcelona 08025, Catalonia, Spain.

*Corresponding author: Francesc.Barquinero@uab.cat

Unitat d'Antropologia Biològica, Departament de Biologia Animal, Biologia Vegetal i Ecologia, Universitat Autònoma de Barcelona, E-08193, Bellaterra, Catalonia, Spain

Keywords: γ-H2AX, biodosimetry, surface model, ionizing radiation,

Biographical Author Notes

Juan S. López, Histocytologist, Ph D student, Department of Animal Biology, Plant Biology and Ecology, Faculty of Biosciencies, Universitat Autònoma de Barcelona (UAB), Bellaterra (Cerdanyola del Vallès), Catalonia, Spain.

Mònica Pujol-Canadell, PhD, Biologist, Postdoctoral research scientist at the Department of Animal Biology, Plant Biology and Ecology, Faculty of Biosciències, Universitat Autònoma de Barcelona (UAB), Bellaterra (Cerdanyola del Vallès), Catalonia, Spain.

Pablo Carrasco, PhD, Physicist, Radiation Physics and Radiation Protection Department, Hospital de la Santa Creu i Sant Pau, Barcelona, Spain.

Pedro Puig, PhD, Mathematician, Professor at the Department of Mathematics and member of the Centre de Recerca Matemàtica, Faculty of Sciences, Universitat Autònoma de Barcelona, Bellaterra (Cerdanyola del Vallés), Catalonia, Spain.

Gemma Armengol, PhD, Biologist, University Professor at the Department of Animal Biology, Plant Biology and Ecology, Faculty of Biosciencies, Universitat Autònoma de Barcelona (UAB), Bellaterra (Cerdanyola del Vallès), Spain.

Montserrat Ribas, Ph. D. in Physics, Medical Physicist, ex-Head of the Department of Radiation Physics and Radiation Protection at the Hospital Santa Creu i Sant Pau, Barcelona, Spain.

Joan-Francesc Barquinero, PhD, Biologist, University Professor at the Department of Animal Biology, Plant Biology and Ecology, Faculty of Biosciencies, Universitat Autònoma de Barcelona (UAB), Bellaterra (Cerdanyola del Vallès), Spain.

ORCID numbers

Juan S. López: 0000-0002-9384-7504
Mònica Pujol-Canadell: 0000-0002-7403-9683
Pedro Puig: 0000-0002-6607-9642
Montserrat Ribas: 0000-0002-5943-145X
Pablo Carrasco: 0000-0002-7893-5813
Gemma Armengol: 0000-0003-2345-1106
Joan-Francesc Barquinero: 0000-0003-0084-5268

ABSTRACT

Introduction: In the event of a radiation accident detecting γ-H2AX foci is being accepted as fast method for triage and dose assessment. However, due to their disappearance kinetics, published calibrations have been constructed at specific post-irradiation times.

Objectives: To develop a surface, or tridimensional, model to estimate doses at times not included in the calibration analysis, and to validate it.

Materials and methods: Calibration data was obtained irradiating peripheral mononucleated cells from one donor with radiation doses ranging from 0 to 3 Gy, and γ -H2AX foci were detected microscopically using a semi-automatic method, at different post-irradiation times from 0.5 to 24 h. For validation, in addition to the above-mentioned donor, blood samples from another donor were also used. Validation was done within the range of doses and post-irradiation times used in the calibration.

Results: The calibration data clearly shows that at each analyzed time, the γ-H2AX foci frequency increases as dose increases, and for each dose this frequency decreases with post-irradiation time. The γ-H2AX foci nucleus distribution was clearly overdispersed, for this reason to obtain bidimensional and tridimensional dose-effect relationships no probability distribution was assumed, and linear and non-linear least squares weighted regression was used. In the two validation exercises for most evaluated samples, the 95% confidence limits of the estimated dose were between ±0.5Gy of the real dose. No major differences were observed between donors.

Conclusion: In case of a suspected overexposure to radiation, the surface model here presented allows a correct dose estimation using γ-H2AX foci as biomarker. The

advantage of this surface model is that it can be used at any post-irradiation time, in our model between 0.5 and 24 h.

1. Introduction

In the case of a radiological accident affecting potentially irradiated victims and to deal with possible adverse health consequences, an initial triage classifying between none, mild, moderate and severe exposed individuals according to the degree of suspected radiation exposure is required. This has to be followed by an accurate dose assessment. To achieve accuracy in triage and dose assessment, both physical and biological based dosimetry are needed.

The analysis of radiation induced chromosomal damage, such as dicentric chromosomes, translocations or micronuclei, has long been used in biological dosimetry in cases of known or suspected exposure to ionizing radiation (IR). The analysis of dicentrics is considered the "gold standard" method, since this biomarker is specific for IR, and its induction shows a good dose-effect correlation, its background is very low (1-2 per thousand), and they are stable enough to be used for dose estimation until months later (IAEA 2011; Grégoire et al. 2018). However, dicentric analysis has some limitations. Although significant progress has been made in automating analysis (Gruel et al. 2013; Romm et al. 2013; Subramanian et al. 2020) it requires trained personnel, and there is a need to culture cells during two days. Rapid biomarkers of exposure have been proposed, most of them based on radiation induced DNA damage (Roch-Lefévre et al. 2010; Rothkamm et al. 2013) and modifications in gene expression (Manning et al. 2013; Abend et al. 2014).

Among the DNA damage induced by IR, DNA double-strand breaks (DSBs) represent the most biologically deleterious type of lesion, and in response to the induced DSBs, the histone H2AX is rapidly phosphorylated on Ser-139 (γ-H2AX). This phosphorylation quickly spreads over several megabases on the adjacent chromatin and can be microscopically detected by fluorescent specific antibodies as γ-H2AX foci (Rogakou et al. 1999). Although some foci may persist over time γ-H2AX is mostly dephosphorylated once DSB repair is achieved (Löbrich et al. 2010). The correlation between the number of DSB produced after irradiation and the number of γ-H2AX foci, makes the number of foci a consistent marker of radiation-induced DSB in single cells (Rothkamm & Löbrich 2003), allowing both the scoring of the foci for quantitative evaluation and the assessment of the disappearance of DSB with post-irradiation times (Rothkamm & Löbrich 2003; Leatherbarrow et al. 2006). The number of γ-H2AX foci induced by IR increases linearly with the radiation dose after both in vitro and in vivo exposure (Löbrich et al. 2005; Leatherbarrow et al. 2006; Rothkamm et al. 2007; Horn et al. 2011; Ivashkevich et al. 2012) Detection of γ-H2AX foci is an assay accepted as biological dosimetry tool (Ainsbury et al. 2014; Moquet et al. 2017).

Rapid blood sample processing for γ-H2AX assay can produce dose estimations within a few hours of receiving a blood sample (Roch-Lefévre et al. 2010; Mandina et al. 2011; Horn et al. 2011; Rothkamm et al. 2013; Ainsbury et al. 2014; Moquet et al. 2017; Lee et al. 2019). For this reason, γ-H2AX assay has a great potential to be used as a rapid triage in a population that has been potentially exposed to IR. In addition, the capacity for batch processing on finger prick blood samples makes the assay ideal for early triage categorization by quantifying radiation-induced foci in peripheral blood mononucleated cells (PBMC) (Moquet et al. 2017; Lee et al. 2019). Additionally, γ-H2AX foci assay

have shown an improved sensitivity to detect exposures to low doses respect classical cytogenetic biomarkers (Ainsbury et al. 2011, Basheerudeen et al. 2017). However, the use of γ-H2AX assay in biodosimetry needs a previous establishment of calibration curves. For this, blood samples from healthy donors are irradiated under monitorized conditions and the yield of γ-H2AX foci is used to generate dose-effect curves. Due to the transitional nature of the phosphorylation, the slopes of these calibration curves show a strong dependency with the post-irradiation time (Roch-Lefévre et al. 2010; Moquet et al. 2017). For this reason, when γ-H2AX assay is used for biological dosimetry purposes, it is mandatory to consider the elapsed time between exposure and blood sample collection, and then to use an appropriate calibration that was established for this particular time (Beels et al. 2010; Roch-Lefévre et al. 2010). This means that laboratories should establish calibration curves for different post-irradiation times.

The aim of the present study is to propose a tri-dimensional or surface model that allows to estimate an exposure using as input the frequency of γ-H2AX foci and any post-irradiation time during the first 24 h after the exposure. To validate this surface model, blinded irradiated samples have been assessed at different post-irradiation times.

2. Material and methods

2.1 Peripheral blood samples and irradiation conditions

Peripheral blood samples from a 54-year-old healthy male were used to construct the dose-effect curve. For the dose-effect curve validation, in addition to the above indicated donor, blood from a 32-year-old healthy female was also used. Blood samples were collected in heparinized tubes. Both donors have no history of exposure to

clastogenic agents. This study has been performed in accordance to institutional, national and international Ethical guidelines. Previous informed consent was obtained for each donor. This project has been approved by Animal and Human Experimentation Ethics Committee of the Universitat Autònoma de Barcelona (Reference: 2624).

Blood samples were mixed (1:1) with 1X phosphate buffered saline (PBS) (Sigma-Aldrich Química, Madrid, Spain) and 6 mL of diluted blood was layered onto 3 mL of Lymphocyte Separation Media (Biowest, Nuaille, France) and then centrifuged at 1200G for 20 min. Isolated PBMCs were washed in 1XPBS and resuspended in RPMI-1640 (Biowest) and kept on ice till the irradiation.

Blood samples were irradiated with 6 MV photon beams from a TrueBeam linear accelerator (Varian Medical Systems, California, USA) located at Hospital de la Santa Creu i Sant Pau, Barcelona. An isocentric setup with two opposed 30 cm X 30 cm fields (0º and 180º) was used to guarantee homogeneous irradiation of blood samples. To irradiate blood samples, tubes were placed inside two holes drilled in a 20 cm X 20 cm polymethyl metacrilate (PMMA) phantom with 20 cm thickness in the direction of the beams. The holes, that fitted tightly the tubes, had been drilled at 2.5 cm distance from the beam axis, and symmetrically placed one another. The PMMA phantom guaranteed almost full scatter conditions, which allowed accurate dose estimations. The attenuation of the carbon fiber table top of the linear accelerator was considered. Dose was prescribed to the average value of the dose delivered to a structure defined by the tube outline. The standard deviation of the dose within the samples, estimated by means of the AAA algorithm as implemented in Eclipse 15.6 treatment planning system (Varian Medical Systems), was 0.8%. LINAC radiation beams were daily checked by means of two independent systems: Daily QA3 (Sun Nuclear, Wisconsin, USA) and Machine Performance Check (Varian Medical Systems). Checks included tests on field size,

beam homogeneity and beam symmetry and stability of the reference dose and the energy. The tolerance level for the absorbed dose test was set at 1.5%. Absorbed dose calibration was performed monthly by means of a PTW 30013 ion chamber traceable to a secondary standard laboratory, CIEMAT, which is the reference laboratory in Spain. The IAEA TRS 398 Code of Practice for absorbed dose determination in external radiotherapy was followed. Before irradiation all samples were warmed up at 37ºC and placed inside the holes of the PMMA phantom. All irradiations were at the same dose rate of 0.5 $Gy \cdot min^{-1}$.

To obtain calibration data, samples were irradiated at 0, 0.25, 0.5, 1, 1.5, 2, 2.5 and 3 Gy. After irradiation, cells were kept on ice during transportation to the laboratory. Cells were incubated at 37 °C for 0.5, 1, 2, 4, 8 and 24 h. To validate the model, two different experiments were done following the same protocol used to obtain calibration data. In the first one, lymphocytes were irradiated at four blinded doses A, B, C and D, that corresponded to 0.5, 0.75, 1 and 1.25 Gy, and evaluated at different post-irradiation times already used for the calibration curves (0.5, 2, 4 and 24 h). In the second experiment, cells were irradiated at five blinded doses E, F, G, H and I, that corresponded to 1, 1.25, 2, 2.75 and 3 Gy, and evaluated at 0.5, 1.5, 3, 6 and 10 hours post-irradiation.

2.2. Immunofluorescence staining and microscopic analysis

First, cell suspensions at a concentration of 35,000 cells·mL-1 were placed in Cytofunnel sample chambers mounted with the Cytoclip slide, containing a poli-D-lysine glass slide. Suspensions were then centrifuged at 500 g for 5 min using a Cytospin centrifuge (Thermo Shandon Cytospin 3, Life sciences International, UK). Then, cells were fixed in 2% paraformaldehyde (Sigma-Aldrich) for 10 min, rinsed with 1XPBS for 5 min, and permeabilized using 1XPBS-0.5% TritonX100 (Sigma-Aldrich)

for 15 min. After two washes with 1XPBS, blocking was carried out for 30 min with a solution containing 1xPBS-0.1% Tweeen20 (Sigma-Aldrich) and 2% fetal bovine serum (GIBCO, Life Technologies, Madrid, Spain). Cells were incubated overnight with a 1:500 dilution of mouse monoclonal anti-γ-H2AX (Ser139) antibody (Abcam, Cambridge, UK) in a humid chamber at 4ºC. Slides were then washed twice with 1XPBS-0.1% tween 20 at RT, 5 min each, and incubated for 1 h at RT with a 1:1000 dilution with the secondary anti-mouse antibody, labeled with cyanine 3 (Cy3) (Amersham Biosciences, Uppsala, Sweden). After washing, slides were rinsed with distilled water, dehydrated with serial ethanol dilutions (70, 85 and 100%) and dried out. Finally, nuclear staining was performed with 4′,6-diamidino-2-phenylindole (DAPI) in Vectashield Mounting Medium (Vector Laboratories, Barcelona, Spain).

Immunofluorescence analysis and image acquisition was performed by automatic microscopy using a Metafer Scanning System (MetaSystems Hard & Software GmbH, Altlussheim, Germany) coupled to a motorized Zeiss AxioImager.Z2. Metafer4 software (MetaSystems Hard & Software GmbH) v 3.10.2. The images were captured using a 63X Plan Apo objective. The foci signals in the selected nuclei were captured using the SpOr filter (red channel). All the SpOr signals were acquired as a z-stack with a total of 10 focal planes and a z-step size of 0.35 mm between plane and automatically analyzed with MetaCyte software (MetaSystems) with a custom-made evaluation algorithm (classifier) optimized previously (Borràs et al 2015). A unique classifier was used to count foci in all samples. The minimum integration time was set to 0.04 s and the maximum one was 0.36 s. The threshold for foci intensity was set to 30% with a maximum gain of 500%. The range area to capture nuclei was established between 30 and 400 μm^2. After automatic capture and analysis, clustered or damaged nuclei were

manually excluded. Both for obtaining the dose-effect relationship and in the two validation exercises, 500 nuclei were recorded in each sample.

2.3. Statistical Analyses

In all cases foci cell distribution was explored using the dispersion index (variance/mean). Dispersion index values greater than one indicate overdispersion, while values less than one indicate underdispersion. To obtain bidimensional and tridimensional dose-effect relationships, linear and non-linear least squares weighted regression was used. Weight-fitting was done using the inverse of variances in all cases, and dose estimation was performed using R (R Core Team 2020). The delta method was used to calculate the 95% confidence limits of the estimated doses (see supplemental file). To compare differences between donors student's t-test was applied.

3. Results

The γ -H2AX foci frequencies obtained for calibration are shown in Table 1. As can be seen at each post-irradiation time evaluated, the frequency of foci per nucleus increases with dose, with values ranging to close to 1 foci per nucleus in the sham irradiated samples to 28.61±0.52 observed 0.5 h after 3 Gy irradiation. Table 1 also shows that for each dose, the foci frequency decreased with post-irradiation time. For the lowest doses, 0.25 and 0.5 Gy, and after 24 h post-irradiation, the foci frequency reached background values, while residual radioinduced foci were still detected at the higher doses: 1, 1.5, 2, 2.5 and 3 Gy. Figure 1 shows foci disappearance kinetics. When the distribution of foci per nucleus was investigated, overdispersion was observed in all samples. The dispersion index did not have a constant value, nor did it show any tendency to increase or decrease with dose or post-irradiation time. When all irradiation doses were considered, higher values of the dispersion index were observed in the middle doses (1,

1.5, and 2 Gy) at all post-irradiation times, while lower values were obtained at 24 h after irradiation.

Results obtained for each of the six post-irradiation times analyzed (0.5, 1, 2, 4, 8 and 24 h) were adjusted to the linear model $Y = c + a \cdot D$ (Figure 2). As can be seen, linear coefficients were higher in the shorter post-irradiation times, 9.64±0.46 at 0.5 h, and then this coefficient steeply decreased achieving the lowest values after 24 h, 1.38±0.19. Considering all doses and all post-irradiation times, foci frequencies observed were fitted to a single surface model, $Y = c \cdot t^{u} + a \cdot t^{v} \cdot D$ (Figure 3). Note that for a defined time the surface model results in a linear equation.

Dose-effect curves adjusted to the linear model as well as surface model were validated in two independent experiments with two donors. The observed results from the first validation exercise are presented in Table 2. For both donors, the foci frequency decreased over post-irradiation time. When both donors were compared, no major differences were obtained neither at each dose nor for each post-irradiation time (Student's t-test). In this first validation exercise, dose-estimations were done using the linear coefficients (Figure 4A), and the surface model (Figure 4B). When linear models were used, in all cases, the 95% confidence intervals of the estimated doses did not include the 0 Gy dose, and in most of the cases, the estimated dose fell within the region of the delivered doses ± 0.5 Gy. This was not the case for 24 h after irradiation. The samples evaluated 24 h after irradiation were those that showed the less accurate estimation. When dose estimations were done using the surface model similar results were obtained. In any of the samples, the estimated doses were 0 Gy, and for most of

the samples the 95% of the confidence interval of the estimated doses fell in the region of ± 0.5 Gy of the delivered dose. When dose estimations using the linear models were compared to those obtained with the surface model, except for 0.75 Gy, dose estimations obtained with the linear models were slightly more accurate. When the linear models were used, the largest difference was observed in the sample irradiated at 0.5 Gy and analyzed 2 h post-irradiation (sample A). For donor 1 the difference between the irradiated dose and the estimated one was 0.60±0.10 Gy using the linear approach and 0.98±0.13 Gy using the surface model, and for donor 2, 0.62±0.10 Gy and 1.04±0.04 Gy respectively.

The results obtained in the second validation exercise are shown in Table 3; in this case, only values obtained after 0.5 h of incubation after 1 and 1.25 Gy irradiation were repeated from the exercise 1. For donor 2 similar frequencies of foci were obtained in the two experiments, around 13 foci per nucleus after 1.25 Gy and 10 after 1 Gy. For donor 1 the obtained frequencies of foci were higher in the second exercise, 15.12±0.25 vs 12.97±0.39 after 1.25 Gy ($p<0.01$, t-test with Welch's correction) and 13.87±0.37 vs 9.28±0.36 after 1 Gy ($p<0.01$). In the second exercise, and contrary to what was observed in the first exercise in which no differences were observed between the two donors, at the initial post-irradiation times (0.5 and 1.5 h) donor 1 showed a tendency to have higher foci frequencies than donor 2. For the remaining post-irradiation times there were no differences, except for 3 Gy and after 10 h post-irradiation where donor 2 showed a higher frequency than donor 1 ($p<0.03$).

Dose-estimations in the second exercise were performed using the surface model (Figure 5). In most of the cases the 95% confidence limits of the estimated doses fell between the ±0.5 Gy interval of the actual dose. Only donor 1 for 1.25 Gy irradiation and after 1.5 h the dose was overestimated (95% interval ranged from 1.81 to 2.02 Gy). In spite of the differences observed between the two donors, when for each dose all estimations were considered, a similar pattern over post-irradiation time is observed. For example, after 1 Gy irradiation, the highest estimated dose was after 1.5 h, and then the estimated doses showed a gradual decrease through post-irradiation time. Similar behavior could be observed after 1.25 Gy. After 1.75 and 2 Gy the estimated doses gradually increased up to 3 h post-irradiation and then gradually decreased.

4. Discussion

After a radiation accident, an estimation of the dose received needs to be provided as soon as possible to support medical decision making and help manage concerns among the potentially exposed individuals. In the last years γ -H2AX assay has been proposed as a very useful triage tool following a recent acute radiation exposure (Barnard et al. 2015), and efforts have been done by the European biodosimetry laboratories network (RENEB) to harmonize the use of this biomarker (Barnard et al. 2015; Kulka et al. 2017; Moquet et al. 2017), or to automate a high throughput system of analysis (Parris et al. 2015; Garty et al. 2015; Durdik et al. 2015; Lee et al. 2019). As it occurs with dicentrics and other biomarkers used in biodosimetry, calibration curves need to be pre-established in each laboratory.

As can be seen in Table 1, the observed frequency of foci at each dose decreased as time after irradiation increased, except at 8 and 24 hours, where no differences were observed between the 0.25 and 0.5 Gy radiation dose. It should be noted that at 8 h both doses (0.25 and 0.5 Gy) differ statistically from 0 Gy. These results indicate that at larger post-irradiation times, and after low dose exposures it would be difficult to precisely estimate the received dose.

All the analyzed samples showed overdispersion (values of the dispersion index higher than 1). Most of the radiation accidents result in partial or heterogeneous exposures, and the use of a discrete probability distribution, such as the Poisson, allows a better estimation of the dose received by the irradiated fraction. This is the case for dicentrics, where zero-inflated or mixed Poisson models have demonstrated their ability to accurately estimate partial and heterogenous exposures (IAEA 2011; Pujol et al. 2016). For γ-H2AX, and considering that the overdispersion in partially irradiated samples is much higher than that observed in uniformly irradiated ones, the zero contaminated Poisson method has been previously used to estimate partial irradiations (Horn et al. 2011). Some authors have described that foci distribution follows a Poisson (Rothkamm & Löbrich 2003; Rothkamm et al. 2007; Lisowska et al. 2013; Zahnreich et al. 2015), many other authors also observed overdispersion in foci distribution (Kato et al. 2006; Lloyd-Smith 2007; Rübe et al. 2008; Martin et al. 2013; Ding et al. 2016; Einbeck et al. 2018). A possible explanation for this overdispersion is that with the present technique we analyze several blood cell types that might differ in their radiation response. An effort should be done in evaluating which discrete probability distribution shows de best match. To deal with the overdispersion some authors have assumed different distributions: negative binomial (Lloyd-Smith 2007; Chilimoniuk et al. 2021), bimodal

Poisson (Kato et al. 2006; Rübe et al. 2008; Martin et al. 2013) or quasi-Poisson models (Errington et al. 2021). In our case, none of the tested distributions gave us satisfactory results, for this reason we did not assume any distribution.

In Table 1 it can also be seen that for sham irradiated samples foci frequency decreased as time of incubation increased. Several tests have been done to elucidate the origin of these foci. Isolation and ice keeping procedures were evaluated (see supplemental data), and while no changes were observed after different times of ice incubation, after lymphocyte isolation there was a significant decrease with incubation time. The lowest value observed in the sham irradiated cells was at 24 h timepoint 0.71 ± 0.04 while the highest one was detected 30 min after irradiation (1.35± 0.06). This is because the foci induced due to isolation cannot be repaired while samples are kept on ice, while after 24 h at 37ºC incubation these foci are repaired. The decrease between 0.5 h and 24 h represents a 50% reduction although in terms of absolute numbers this represents less than 1 foci per cell reduction. Several background foci values have been previously described, these ranged from 0 to 1.05 foci per nucleus (Beels et al. 2010; Mandina et al. 2011; K. Rothkamm et al. 2013; Chaurasia et al. 2021). In addition, to the interindividual differences and the way foci are scored (manually or semi-automatic), our results suggest that in a radiation accident or in an intercomparison, when lymphocytes are isolated just before fixing the sample, a small amount of foci can be produced. However, our study suggests that this induction should not be higher than 1 foci per nucleus. This effect should only be considered when blood samples are obtained after 24 or more hours.

Dose-effect curves based on γ-H2AX foci has been classically adjusted to the linear model $Y = c+a \cdot D$. (Andrievski & Wilkins 2009; Redon et al. 2009; Roch-Lefévre et al. 2010; Mandina et al. 2011; Horn et al. 2011; Lisowska et al. 2013; Rothkamm et al. 2013; Zahnreich et al. 2015; Ding et al. 2016; Moquet et al. 2017; Lee et al. 2019; Chaurasia et al. 2021). In the present study adjustment to the linear model can be seen in Figure 2, which shows that slope of the curves decreases over time after irradiation. This is due to the fact that foci frequencies reach the maximum 30 min after irradiation and decrease progressively with time after irradiation. In the present study slopes range from 9.64 ± 0.45 after 0.5 h to 1.39 ± 0.29 after 24 h. Since published data show a great variability in different methodological steps, direct comparisons with published calibration data can be misleading. However, if only curves obtained after 0.5 and 24 h are considered, the slopes published range from 10-15 to 1-2 foci per nucleus and per Gy respectively. These values are in agreement with the ones obtained in the present study (Redon et al. 2009; Roch-Lefévre et al. 2010; Mandina et al. 2011; Lisowska et al. 2013; Rothkamm et al. 2013; Chaurasia et al. 2021).

After a radiation accident a relatively wide window of time lapse to collect the blood sample exists, and some authors agree that this window could fit in the interval of 8-24 (Roch-Lefévre et al. 2010; Barnard et al. 2015; Moquet et al. 2017). In case of an accident, and to perform reliable dose estimations, blood samples should be collected at the same timepoints at which the calibrations curves have been elaborated. However, to collect samples at specific times can represent a logistic problem difficult to solve. In the present study this problem was addressed by proposing a surface model. The model assumes that the moment of exposure is known, so blood can be collected any time between 0.5 and 24 h.

Two independent validation exercises were done. In the first one, post-irradiation times of sample processing were the same of the ones used to construct both the linear curves and the surface model. Although estimations using the linear curves were a little more accurate than those estimated using the surface model, all of them were correctly placed between >0 Gy and <1.5 Gy. Values further of the actual doses were those assessed 24 h after irradiation. This is probably due to the fact that around 15 to 24 h post-irradiaton the frequency of foci decreases very lightly (Figure 1), and that at these times the foci frequency induced at different doses tend to converge to low values, in our case about 1 to 6 foci per nuclei. These two conditions produce that in longer times the slopes are fairly flat, and consequently small changes in foci frequencies have higher impact in the estimated dose. In the second exercise, and because the timepoints chosen were different to the ones used to construct the dose-effect curves, dose-estimations were performed only with the surface model. The estimated doses were quite accurate, and only two dose estimations for donor 1 were out of the ±0.5 Gy interval. This result indicates the robustness of the surface model and its applicability.

Some authors have detected a strong interindividual difference in the induction of γ - H2AX foci, which compromises its use as a radiation biomarker (Hamasaki et al. 2007; Ismail et al. 2007; Andrievski & Wilkins 2009). In the present study, the results obtained by the two donors and in the two validation exercises were very similar, even at longer post-irradiation times. When estimated doses were evaluated, something noticeable is that for most of the doses a similar pattern along post-irradiation time was observed in both donors. A possible explanation of this behavior is that small changes in some of the initial steps of the protocol when the repair kinetics is faster (during the first

two hours), like temperature monitoring or time precision, can slightly affect the foci observed.

In conclusion, the surface model here presented, that comprises the first 24 h post-irradiation, allows to reliably estimate the received dose, with a similar accuracy than linear dose-effect curves but with the advantage that dose estimation can be assessed at any post-irradiation time.

Acknowledgements

This work received financial support from the Spanish Consejo de Seguridad Nuclear (BOE-A-2019-311). MR, PC, GA and JFB are part of a SGR recognized by the Generalitat de Catalunya (2017SGR0255).

Disclosure statement

No conflict of interest was reported by the authors.

References

Abend M, Azizova T, Müller K, Dörr H, Senf S, Kreppel H, Rusinova G, Glazkova I, Vyazovskaya N, Schmidl D, et al. 2014. Gene expression analysis in mayak workers with prolonged occupational radiation exposure. Health Phys. 106(6):664–676.

Ainsbury EA, Bakhanova E, Barquinero JF, Brai M, Chumak V, Correcher V, Darroudi F, Fattibene P, Gruel G, Guclu I, et al. 2011. Review of retrospective dosimetry techniques for external ionising radiation exposures. Radiat Prot Dosimetry.147(4):573-592.

Ainsbury EA, Al-Hafidh J, Bajinskis A, Barnard S, Barquinero JF, Beinke C, De Gelder V, Gregoire E, Jaworska A, Lindholm C, et al. 2014. Inter- and intra-laboratory comparison of a multibiodosimetric approach to triage in a simulated, large scale radiation emergency. Int J Radiat Biol. 90(2):193–202.

Andrievski A, Wilkins RC. 2009. The response of γ-H2AX in human lymphocytes and lymphocytes subsets measured in whole blood cultures. Int J Radiat Biol. 85(4):369–376.

Barnard S, Ainsbury EA, Al-Hafidh J, Hadjidekova V, Hristova R, Lindholm C, Monteiro Gil O, Moquet J, Moreno M, Rößler U, et al. 2015. The first γ -H2AX biodosimetry intercomparison exercise of the developing european biodosimetry network RENEB. Radiat Prot Dosimetry. 164(3):265–270.

Basheerudeen SAS, Kanagaraj K, Jose MT, Ozhimuthu A, Paneerselvam S, Pattan S, Joseph S, Raavi V, Perumal V. 2017. Entrance surface dose and induced DNA damage in blood lymphocytes of patients exposed to low-dose and low-dose-rate X-irradiation during diagnostic and therapeutic interventional radiology procedures. Mutat Res. 818:1-6.

Beels L, Werbrouck J, Thierens H. 2010. Dose response and repair kinetics of γ-H2AX foci induced by in vitro irradiation of whole blood and T-lymphocytes with X-and γ-radiation. Int J Radiat Biol. 86(9):760–768

Borràs M, Armengol G, De Cabo M, Barquinero JF, Barrios L. 2015. Comparison of methods to quantify histone H2AX phosphorylation and its usefulness for prediction of radiosensitivity. Int J Radiat Biol. 91(12):915-24.

Chaurasia RK, Bhat NN, Gaur N, Shirsath KB, Desai UN, Sapra BK. 2021. Establishment and multiparametric-cytogenetic validation of 60Co-gamma-ray induced, phospho-gamma-H2AX calibration curve for rapid biodosimetry and triage management during radiological emergencies. Mutat Res - Genet Toxicol Environ Mutagen 866. 503354

Chilimoniuk J, Gosiewska A, Słowik J, Weiss R, Deckert PM, Rödiger S, Burdukiewicz M. 2021. countfitteR: efficient selection of count distributions to assess DNA damage. Ann Transl Med. 9(7):528–528.

Ding D, Zhang Y, Wang J, Wang X, Fan D, He L, Zhang X, Gao Y, Li Q, Chen H. 2016. γ-H2AX/53BP1/pKAP-1 foci and their linear tracks induced by in vitro exposure to radon and its progeny in human peripheral blood lymphocytes. Sci Rep. 6. 38295

Durdik M, Kosik P, Gursky J, Vokalova L, Markova E, Belyaev I. 2015. Imaging flow cytometry as a sensitive tool to detect low-dose-induced DNA damage by analyzing 53BP1 and γH2AX foci in human lymphocytes. Cytom Part A. 87(12):1070–1078.

Einbeck J, Ainsbury EA, Sales R, Barnard S, Kaestle F, Higueras M. 2018. A statistical framework for radiation dose estimation with uncertainty quantification from the γ-H2AX assay. PLoS One. 13(11):e0207464.

Errington A, Einbeck J, Cumming J, Rössler U, Endesfelder D. 2021. The effect of data aggregation on dispersion estimates in count data models. Int J Biostat. 0(0).

Garty G, Bigelow AW, Repin M, Turner HC, Bian D, Balajee AS, Lyulko O V., Taveras M, Yao YL, Brenner DJ. 2015. An automated imaging system for radiation biodosimetry. Microsc Res Tech. 78(7):587–598.

Grégoire E, Roy L, Buard V, Delbos M, Durand V, Martin-Bodiot C, Voisin Pascale, Sorokine-Durm I, Vaurijoux A, Voisin Philippe, et al. 2018. Twenty years of FISH-based translocation analysis for retrospective ionizing radiation biodosimetry. Int J Radiat Biol. 94(3):248–258.

Gruel G, Grégoire E, Lecas S, Martin C, Roch-Lefevre S, Vaurijoux A, Voisin Pascale, Voisin Philippe, Barquinero JF. 2013. Biological dosimetry by automated dicentric scoring in a simulated emergency. Radiat Res. 179(5):557–569.

Hamasaki K, Imai K, Nakachi K, Takahashi N, Kodama Y, Kusunoki Y. 2007. Short-term culture and γH2AX flow cytometry determine differences in individual radiosensitivity in human peripheral T lymphocytes. Environ Mol Mutagen. 48(1):38–47.

Horn S, Barnard S, Rothkamm K. 2011. Gamma-H2AX-based dose estimation for whole and partial body radiation exposure. PLoS One. 6(9): e25113

IAEA. 2000. Absorbed Dose Determination in External Beam Radiotherapy. Vienna, Austria: International Atomic Energy.

IAEA. 2011. Cytogenetic Dosimetry: Applications in Preparedness for and Response to Radiation Emergencies. Vienna, Austria: International Atomic Energy.

Ismail IH, Wadhra TI, Hammarsten O. 2007. An optimized method for detecting gamma-H2AX in blood cells reveals a significant interindividual variation in the gamma-H2AX response among humans. Nucleic Acids Res. 35(5).e36

Ivashkevich A, Redon CE, Nakamura AJ, Martin RF, Martin OA. 2012. Use of the γ-H2AX assay to monitor DNA damage and repair in translational cancer research. Cancer Lett. 327(1–2):123–133.

Kato TA, Nagasawa H, Weil MM, Little JB, Bedford JS. 2006. Levels of γ-H2AX foci after low-dose-rate irradiation reveal a DNA DSB rejoining defect in cells from human ATM heterozygotes in two AT families and in another apparently normal individual. Radiat Res. 166(3):443–453.

Kulka U, Abend M, Ainsbury E, Badie C, Barquinero JF, Barrios L, Beinke C, Bortolin E, Cucu A, De Amicis A, et al. 2017. RENEB–Running the European Network of biological dosimetry and physical retrospective dosimetry. Int J Radiat Biol. 93(1):2–14.

Leatherbarrow EL, Harper J V., Cucinotta FA, O'Neill P. 2006. Induction and quantification of γ-H2AX foci following low and high LET-irradiation. Int J Radiat Biol. 82(2):111–118.

Lee Y, Wang Q, Shuryak I, Brenner DJ, Turner HC. 2019. Development of a high-throughput γ-H2AX assay based on imaging flow cytometry. Radiat Oncol. 14(150).

Lisowska H, Wegierek-Ciuk A, Banasik-Nowak A, Braziewicz J, Wojewodzka M, Wojcik A, Lankoff A. 2013. The dose-response relationship for dicentric chromosomes and γ-H2AX foci in human peripheral blood lymphocytes: Influence of temperature during exposure and intra- and inter-individual variability of donors. Int J Radiat Biol. 89(3):191–199.

Lloyd-Smith JO. 2007. Maximum likelihood estimation of the negative binomial dispersion parameter for highly overdispersed data, with applications to infectious diseases. PLoS One. 2(2) e180.

Löbrich M, Rief N, Kühne M, Heckmann M, Fleckenstein J, Rübe C, Uder M. 2005. In vivo formation and repair of DNA double-strand breaks after computed tomography examinations. Proc Natl Acad Sci U S A.102(25):8984–8989.

Löbrich M, Shibata A, Beucher A, Fisher A, Ensminger M, Goodarzi AA, Barton O, Jeggo PA. 2010. γH2AX foci analysis for monitoring DNA double-strand break repair: Strengths, limitations and optimization. Cell Cycle. 9(4):662–669.

Mandina T, Roch-Lefvre SH, Voisin Pascale, González JE, Lamadrid AI, Romero I, García O, Voisin Philippe, Roy L. 2011. Dose-response relationship of γ-H2AX foci induction in human lymphocytes after X-rays exposure. Radiat Meas. 46(9):997–999.

Manning G, Kabacik S, Finnon P, Bouffler S, Badie C. 2013. High and low dose responses of transcriptional biomarkers in ex vivo X-irradiated human blood. Int J Radiat Biol. 89(7):512–522.

Martin OA, Ivashkevich A, Choo S, Woodbine L, Jeggo PA, Martin RF, Lobachevsky P. 2013. Statistical analysis of kinetics, distribution and co-localisation of DNA repair foci in irradiated cells: Cell cycle effect and implications for prediction of radiosensitivity. DNA Repair (Amst) 12(10):844–855.

Moquet J, Barnard S, Staynova A, Lindholm C, Monteiro Gil O, Martins V, Rößler U, Vral A, Vandevoorde C, Wojewódzka M, Rothkamm K. 2017. The second gamma-H2AX assay inter-comparison exercise carried out in the framework of the European biodosimetry network (RENEB). Int J Radiat Biol. 93(1):58–64.

Parris CN, Adam Zahir S, Al-Ali H, Bourton EC, Plowman C, Plowman PN. 2015. Enhanced γ-H2AX DNA damage foci detection using multimagnification and extended depth of field in imaging flow cytometry. Cytom Part A. 87(8):717–723.

Pujol M, Barrios L, Puig P, Caballín MR, Barquinero JF. 2016. A New Model for Biological Dose Assessment in Cases of Heterogeneous Exposures to Ionizing Radiation. Radiat Res. 185(2):151–162.

R Core Team. 2020. R: A language and environment for statistical computing. Vienna, Austria.

Redon CE, Dickey JS, Bonner WM, Sedelnikova OA. 2009. γ-H2AX as a biomarker of DNA damage induced by ionizing radiation in human peripheral blood lymphocytes and artificial skin. Adv Sp Res. 43(8):1171–1178.

Roch-Lefévre S, Mandina T, Voisin Pascale, Gëatan G, Mesa JEG, Valente M, Bonnesoeur P, García O, Voisin Philippe, Roy L. 2010. Quantification of γ-H2AX Foci in human lymphocytes: A method for biological dosimetry after ionizing radiation exposure. Radiat Res. 174(2):185–194

Rogakou EP, Boon C, Redon C, Bonner WM. 1999. Megabase chromatin domains involved in DNA double-strand breaks in vivo. J Cell Biol. 146(5):905–915.

Romm H, Ainsbury E, Barnard S, Barrios L, Barquinero JF, Beinke C, Deperas M, Gregoire E, Koivistoinen A, Lindholm C, et al. 2013. Automatic scoring of dicentric chromosomes as a tool in large scale radiation accidents. Mutat Res - Genet Toxicol Environ Mutagen. 756(1–2):174–183.

Rothkamm K, Balroop S, Shekhdar J, Fernie P, Goh V. 2007. Leukocyte DNA damage after multi-detector row CT: A quantitative biomarker of low-level radiation exposure. Radiology. 242(1):244–251.

Rothkamm Kai, Barnard S, Ainsbury EA, Al-hafidh J, Barquinero JF, Lindholm C, Moquet J, Perälä M, Roch-Lefèvre S, Scherthan H, et al. 2013. Manual versus automated γ-H2AX foci analysis across five European laboratories: Can this assay be used for rapid biodosimetry in a large scale radiation accident? Mutat Res - Genet Toxicol Environ Mutagen. 756(1–2):170–173.

Rothkamm K., Horn S, Scherthan H, Rößler U, De Amicis A, Barnard S, Kulka U, Lista F, Meineke V, Braselmann H, et al. 2013. Laboratory intercomparison on the γ-H2AX foci assay. Radiat Res. 180(2):149–155.

Rothkamm K, Löbrich M. 2003. Evidence for a lack of DNA double-strand break repair in human cells exposed to very low x-ray doses. Proc Natl Acad Sci U S A. 100(9):5057–5062.

Rübe CE, Grudzenski S, Kühne M, Dong X, Rief N, Löbrich M, Rübe C. 2008. DNA double-strand break repair of blood lymphocytes and normal tissues analysed in a preclinical mouse model: Implications for radiosensitivity testing. Clin Cancer. 14(20):6546–6555.

Subramanian U, O'Brien B, McNamara M, Romanyukha L, Bolduc DL, Olsen C, Blakely WF. 2020. Automated Dicentric Aberration Scoring for Triage Dose Assessment: 60Co Gamma Ray Dose-response at Different Dose Rates. Health Phys. 119(1):52–58.

Zahnreich S, Ebersberger A, Kaina B, Schmidberger H. 2015. Biodosimetry based on γ-H2AX quantification and cytogenetics after partial-and total-body irradiation during fractionated radiotherapy. Radiat Res. 183(4):432–446.

Figure legends

Figure 1. In the irradiated samples used to obtain calibration data, kinetics disappearance of γ-H2AX foci through post-irradiation time: For each dose lines shows the one-phase decay approximation.

Figure 2. From the calibration data, observed frequencies of γ-H2AX foci ±SE, and linear dose-effect curves for each post-irradiation time. Obtained slopes are; for 0.5 h Y= 1.47±0.25 + 9.46±0.46D; for 1 hr Y= 1.01±0.28 + 8.58±0.60D; for 2 h Y= 0.89±0.20 + 7.33±0.44D; for 4 h Y= 0.91±0.19 + 4.16±0.34D; for 8 h Y= 0.63±0.56 + 2.06±0.40D; for 24 h Y= 0.26±0.14 + 1.38±0.19D

Figure 3. Surface model obtained when all calibration data was considered jointly. The obtained calibration is $Y = c \cdot t^{u} + a \cdot t^{v} \cdot D$ where c=1.15±0.17; u=-0.29±0.11; a=7.73±0.33; v=-0.50±0.04.

Figure 4. Estimated doses in the first validation exercise. For each donor (black circles donor 1, and black squares donor 2) and dose (0.5, 0.75, 1, and 1.25 Gy) estimations after 0.5, 2, 4 and 24 h are represented consecutively. Horizontal lines represent the

actual doses, and the shaded area represents the ±0.5Gy of the actual dose. A, estimated doses using the linear dose-effect curves. B, estimated doses using the surface model.

Figure 5. Estimated doses in the second validation exercise. For each donor (black circles donor 1, and black squares donor 2) and dose (1, 1.25, 2, 2.75, and 3 Gy) estimations after 0.5, 1.5, 3, 6 and 10 h are represented consecutively. Horizontal lines represent the actual doses, and the shaded area represents the ±0.5Gy of the actual dose. A, estimated doses using the linear dose-effect curves. B, estimated doses using the surface model.

Table 1: Frequency of foci observed for dose and post irradiation time.

Dose (Gy)	Post-irradiation time (h)											
	0.5		1		2		4		8		24	
	y ± SE	s^2/y	y ± SE	s^2/y	y ± SE	s^2/y	y ± SE	s^2/y	y ± SE	s^2/y	y ± SE	s^2/y
0	1.35±0.06	1.45	0.86±0.05	1.61	0.80±0.05	1.29	0.84±0.05	1.48	0.68±0.04	1.26	0.71±0.04	1.33
0.25	5.75±0.28	6.93	5.01±0.27	7.30	4.10±0.20	4.79	2.99±0.18	5.55	1.44±0.10[a]	3.63	0.83±0.07[a]	2.68
0.5	7.98±0.38	9.07	7.85±0.24	3.79	5.95±0.25	5.45	3.84±0.20	5.31	1.57±0.13[a]	5.31	0.86±0.08[a]	3.56
1	11.70±0.40	6.87	9.37±0.38	7.86	7.73±0.34	7.51	4.40±0.28	9.02	2.02±0.14	5.11	1.89±0.12	4.11
1.5	14.43±0.47	7.67	12.83±0.42	6.83	10.62±0.39	7.11	5.86±0.26	5.89	2.30±0.18	7.30	2.12±0.17	6.92
2	22.16±0.61	8.45	18.11±0.59	9.54	17.54±0.51	7.28	9.22±0.43	9.94	3.30±0.23	8.18	3.00±0.20	6.34
2.5	26.36±0.55	5.64	23.06±0.57	7.12	20.13±0.52	6.77	10.89±0.40	7.39	7.20±0.27	4.89	4.15±0.22	5.86
3	28.61±0.52	4.81	25.06±0.48	4.65	21.29±0.43	4.29	15.16±0.45	6.79	10.73±0.35	5.73	6.25±0.25	5.09

Frequency ± standard error (y ± SE) and dispersion index= variance/mean(s^2/y).[a] indicates non statistically significant differences between foci frequencies of the previous timepoint and the current one.

Table 2: Frequency of foci in the first validation exercise

Sample	Post-irradiation time (h)							
	0.5		2		4		24	
	y ± SE		y ± SE		y ± SE		y ± SE	
	Donor 1	Donor 2	Donor 1	Donor 2	Donor 1	Donor 2	Donor 1	Donor 2
A	8.69±0.30	8.40±0.29	6.30±0.29	6.63±0.27	4.29 ± 0.24	4.07±0.93	0.95 ± 0.11	0.93±0.10
B	7.24±0.29	7.73±0.30	5.27±0.23	5.41±0.22	4.49 ± 0.25	4.47±0.25	1.06 ± 0.13	1.01±0.12
C	9.28±0.36	9.57±0.33	6.01±0.29	6.19±0.30	4.94 ± 0.25	4.95±0.22	1.20 ± 0.13	1.21±0.10
D	12.97±0.39	13.50±0.35	9.27±0.34	9.58±0.33	5.80 ± 0.24	6.03±0.25	1.37±0.11	1.38±0.12

A. B.C and D correspond to blinded samples that were irradiated with 0.75. 0.5. 1.00 and 1.25 Gy.

Table 3: Frequency of foci in the second validation exercise

Sample	Post-irradiation time (h)									
	0.5		1.5		3		6		10	
	y ± SE		y ± SE		y ± SE		y ± SE		y ± SE	
	Donor 1	Donor 2	Donor 1	Donor 2	Donor 1	Donor 2	Donor 1	Donor 2	Donor 1	Donor 2
E	15.12±0.50	13.00±0.40*	13.80±0.48	10.33±0.41*	6.05±0.23	5.50±0.21	3.38±0.20	3.44±0.19	2.55±0.15	2.89±0.19
F	19.06±0.47	15.86±0.47*	15.35±0.44	12.80±0.41*	12.15±0.36	9.39±0.40*	6.17±0.22	5.87±0.28	4.04±0.20	3.84±0.22
G	13.87±0.37	10.43±0.33*	10.21±0.38	8.07±0.38*	5.04±0.29	4.31±0.26	2.85±0.12	2.59±0.16	1.90±0.12	1.95±0.15
H	27.18±0.30	26.69±0.41	16.73±0.45	15.95±0.44	12.92±0.39	13.43±0.47	9.06±0.35	9.22±0.35	7.06±0.24	7.15±0.24
I	28.95±0.31	26.64±0.20*	17.38±0.46	17.79±0.50	15.98±0.47	16.02±0.42	11.28±0.44	12.00±0.43	7.12±0.24	7.96±0.30**

E,. F,.G, H and I and D correspond to the irradiated samples to doses of 1.25, 2, 1, 2.75 and 3 Gy. Significant differences between both donors, * P<0.01, **p<0.03 (Student's t-test).

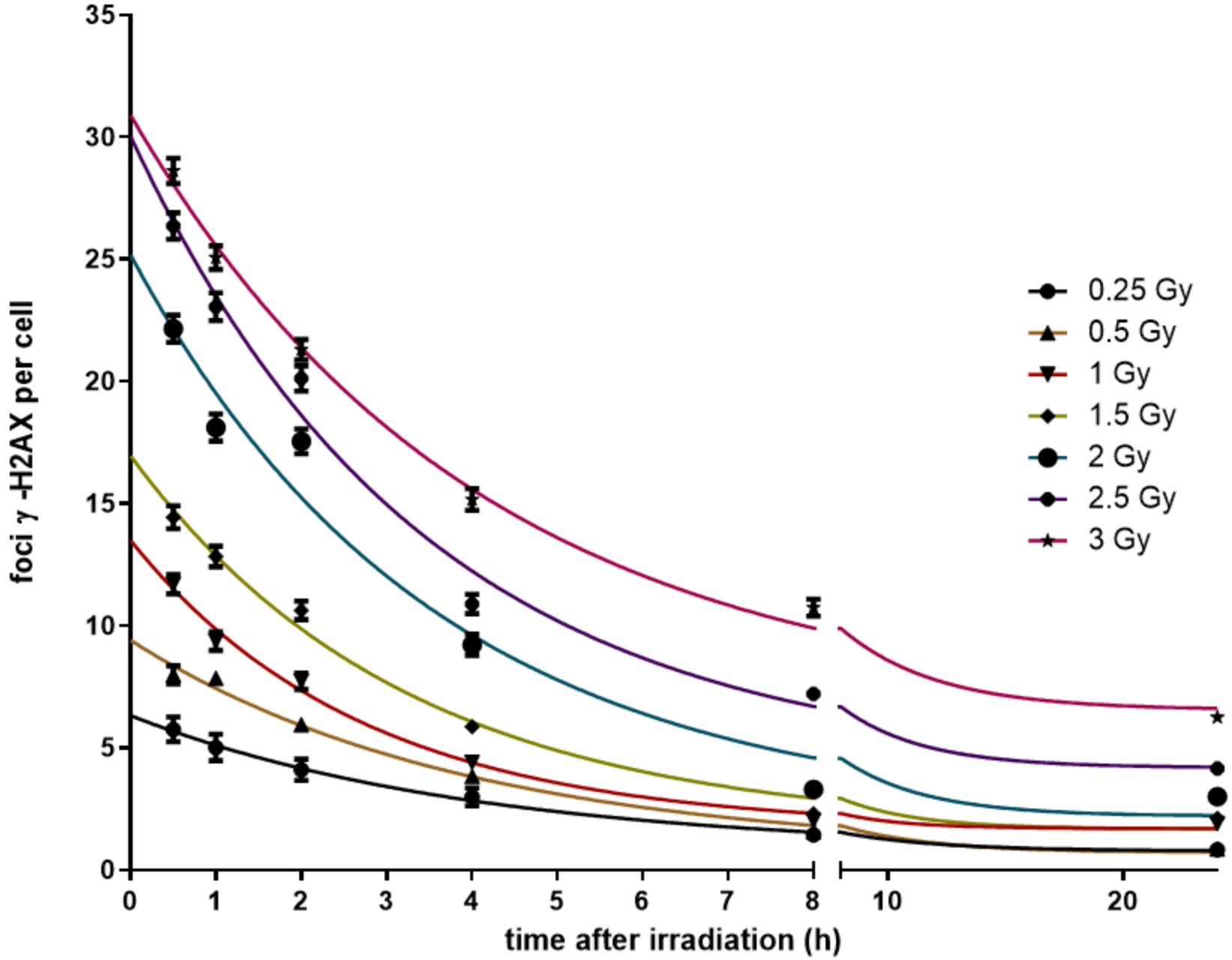
foci γ -H2AX per cell
time after irradiation (h)
0.25 Gy
0.5 Gy
1 Gy
1.5 Gy
2 Gy
2.5 Gy
3 Gy
0
5
10
15
20
25
30
35
0
1
2
3
4
5
6
7
8
10
20

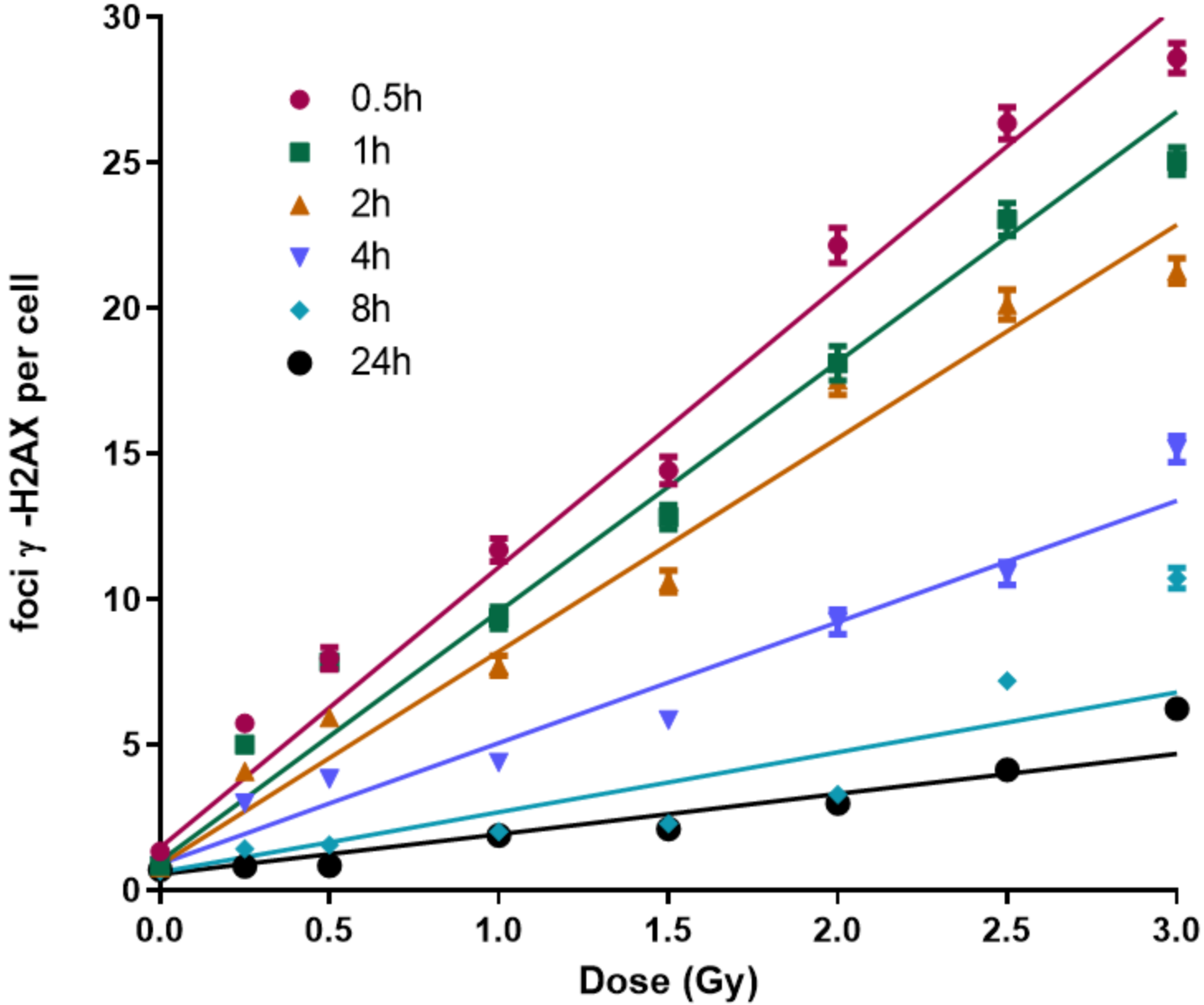
30
25
20
15
10
5
0
foci γ -H2AX per cell
0.5h
1h
2h
4h
8h
24h
0.0
0.5
1.0
1.5
2.0
2.5
3.0
Dose (Gy)

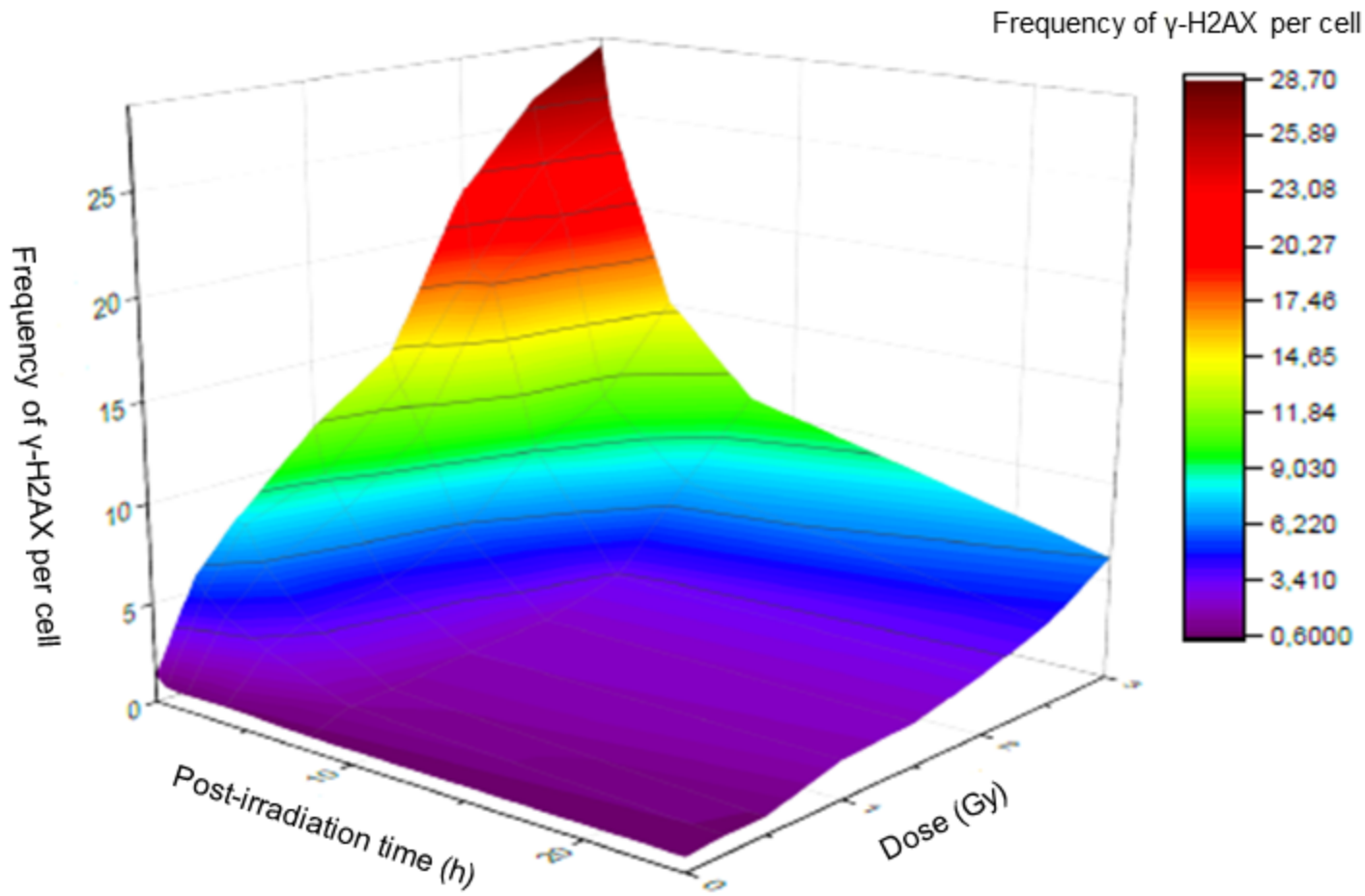
Frequency of γ-H2AX per cell
28,70
25,89
23,08
20,27
17,46
14,65
11,84
9,030
6,220
3,410
0,6000
Frequency of γ-H2AX per cell
25
20
15
10
5
0
Post-irradiation time (h)
Dose (Gy)

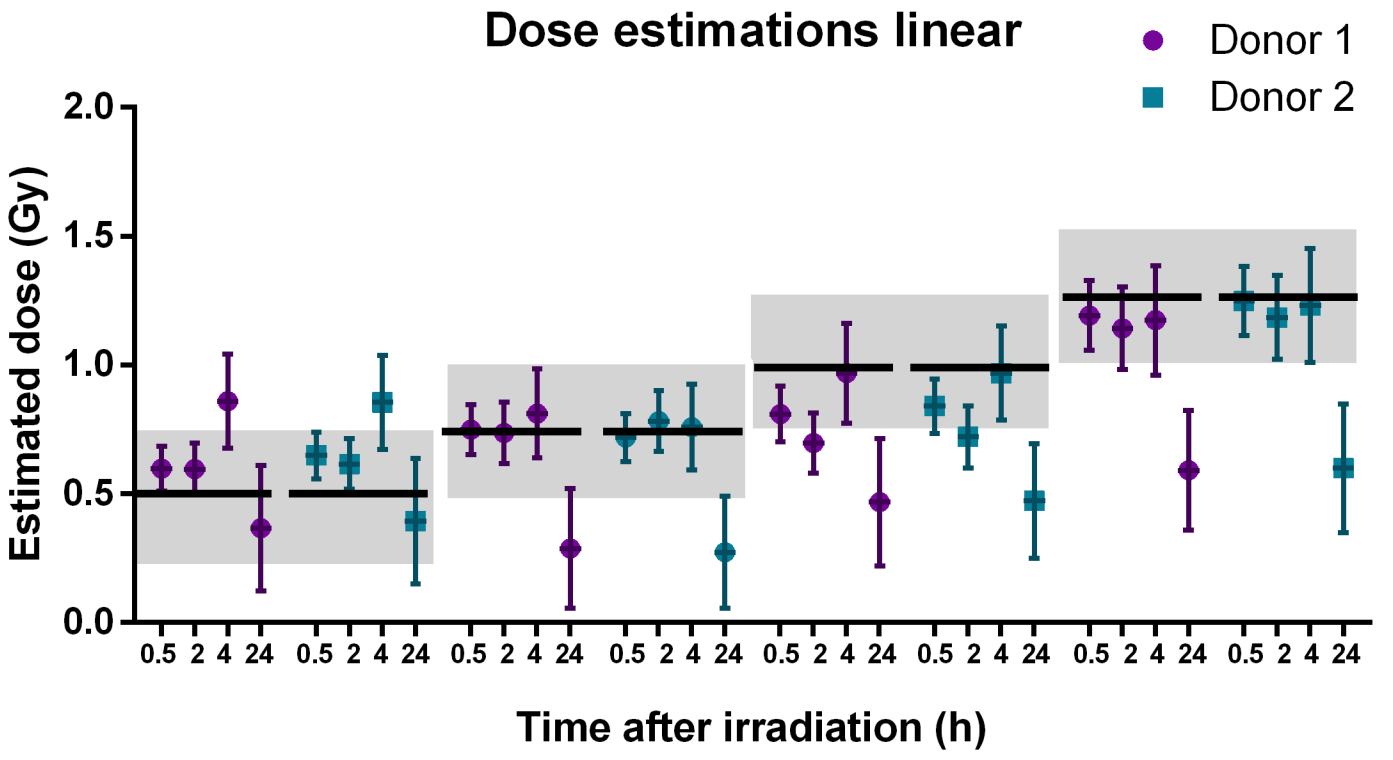
Dose estimations linear
Donor 1
Donor 2
Estimated dose (Gy)
2.0
1.5
1.0
0.5
0.0
0.5 2 4 24 0.5 2 4 24 0.5 2 4 24 0.5 2 4 24 0.5 2 4 24 0.5 2 4 24 0.5 2 4 24
Time after irradiation (h)

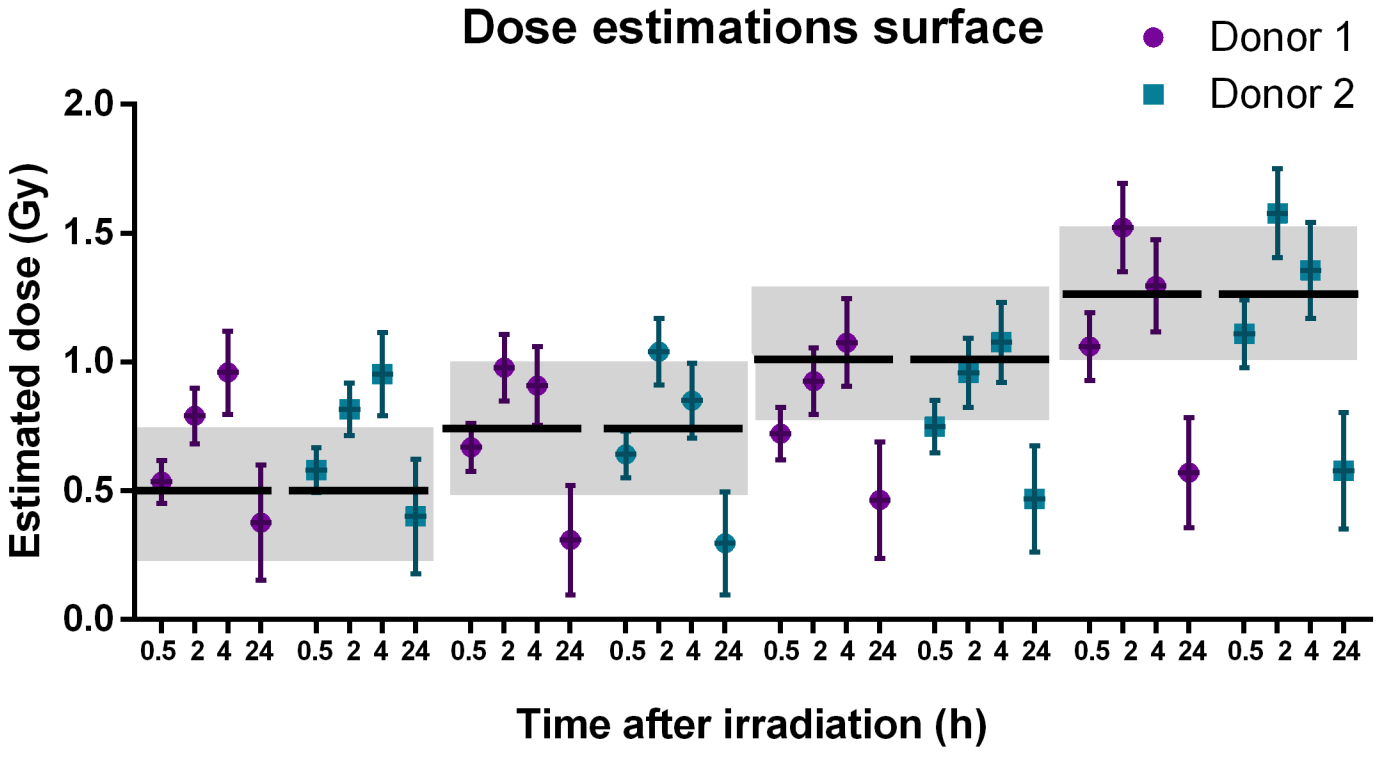
Dose estimations surface
Donor 1
Donor 2
Estimated dose (Gy)
2.0
1.5
1.0
0.5
0.0
0.5 2 4 24 0.5 2 4 24 0.5 2 4 24 0.5 2 4 24 0.5 2 4 24 0.5 2 4 24 0.5 2 4 24
Time after irradiation (h)

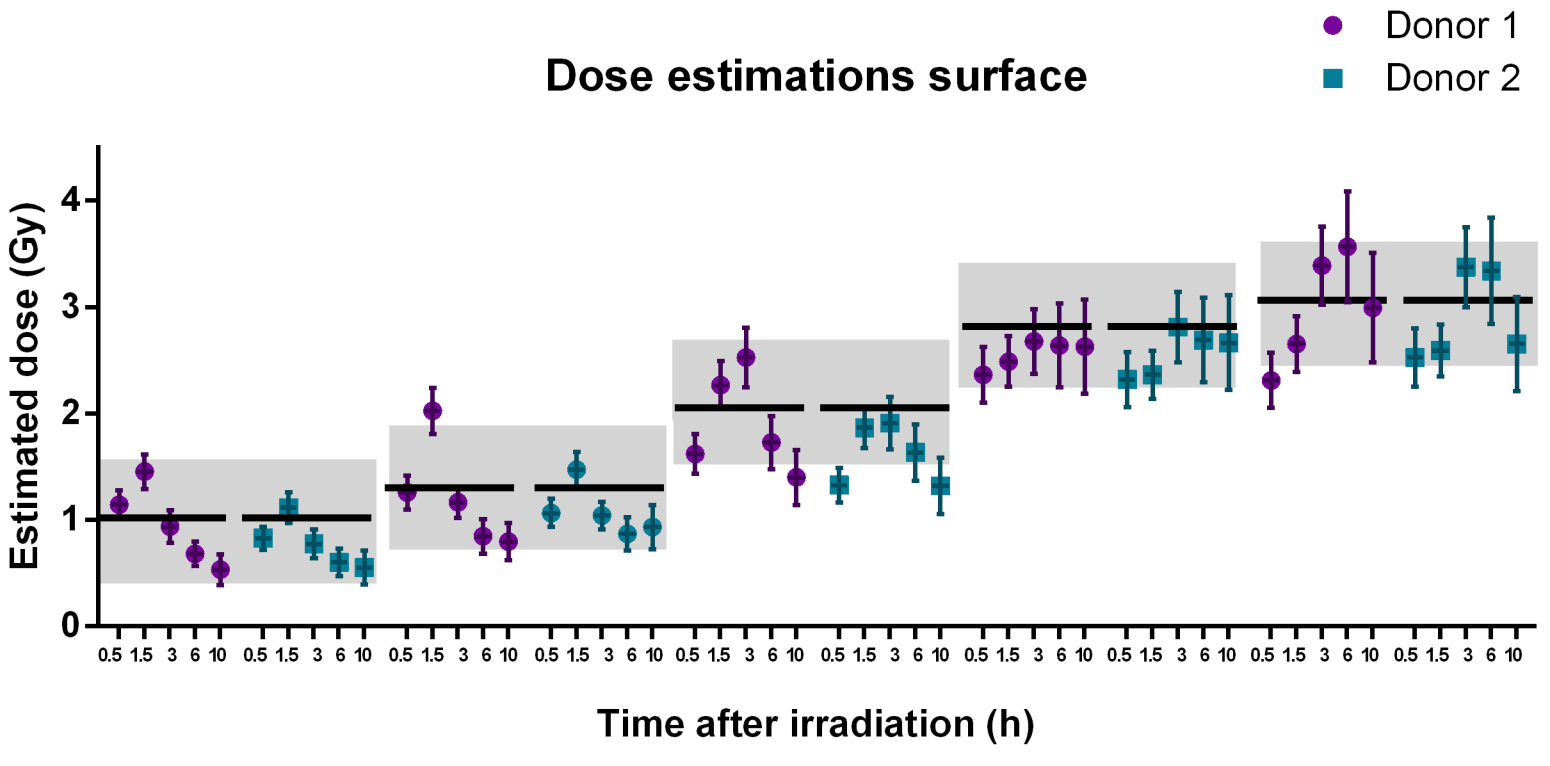
Donor 1
Donor 2
Dose estimations surface
Estimated dose (Gy)
0
1
2
3
4
0.5 1.5 3 6 10 0.5 1.5 3 6 10 0.5 1.5 3 6 10 0.5 1.5 3 6 10 0.5 1.5 3 6 10 0.5 1.5 3 6 10 0.5 1.5 3 6 10 0.5 1.5 3 6 10 0.5 1.5 3 6 10 0.5 1.5 3 6 10
Time after irradiation (h)